Regional Climate Simulation for Korea using Dynamic Downscaling and Statistical Adjustment

J.-H. OH, T. KIM

Department of Environmental Atmospheric Sciences, Pukyong National University, Busan, Korea

M.-K. KIM

Department of Atmospheric Science, Kongju National University, Chungnam, Korea

S.-H. LEE

Department of Geography, Konkuk University, Seoul, Korea

S.-K. MIN and W.-T. KWON

Meteorological Research Institute, the Korea Meteorological Administration, Seoul, Korea

(Manuscript received 18 June 2003, in final form 18 June 2004)

Abstract

Recently the regional impact assessment due to global warming is one of the urgent tasks to every country in the world, under the circumstances of increasing carbon dioxide in the atmosphere. This assessment must include not only meteorological factors, such as surface air temperature and precipitation, etc., but also the response of the local ecosystem. Based on a previous study, for example, it has been known that *Phyllostachys'* habitation, which is one of the bamboo species popular in Korea, is quite sensitive to temperature change, in particular during the winter season. Thus, adequate climate information is essential to derive a solid conclusion on the regional impact assessment for future climate change.

In this study, we adopted a dynamical downscaling technique to get regional future climate information, with the regional climate model (MM5, Pennsylvania State University/National Center for Atmospheric Research mesoscale model) from the Max-Planck Institute for Meteorology Models and Data Group's Atmosphere-Ocean General Circulation Model (AOGCM) ECAHM4, and HOPE-G (ECHO-G) simulation for future climate, based on future greenhouse gas (GHG) emission scenario of the Intergovernmental Panel on Climate Change (IPCC) Special Report on Emission Scenarios (SRES) A2. Through this nesting process we got reasonable regional climate change information. However, we found a couple of systematic differences, such as a cold bias in the surface air temperature, simulated by MM5 compared to that by the AOGCM ECHO-G. This cold bias may cause to loose credibility on the future climate scenario to the impact assessment studies. Accordingly, we introduced a transfer function to correct the systematic bias of the dynamic model in the regional-scale, and to predict the regional cli-

Corresponding author: Jai-Ho Oh, Integrated Climate System Modeling Group, Department of Environmental Atmospheric Sciences, Pukyong National University, 599-1 Daeyeon3-dong, Nam-gu, Busan 608-737, South Korea.
E-mail: jhoh@pknu.ac.kr

mate from large-scale predictors. These transfer functions are obtained from the daily mean temperature of 17 surface observation stations in Korea for 10 years from 1992 to 2001, and 10-year simulation data obtained from regional climate model (RCM) for each mode of EOFA to correct the systematic bias of RCM data.

With these transfer functions, we can correct the RMS error of the daily mean temperature in RCM as much as 47.6% in winter and 86.5% in summer. After dynamical downscaling and statistical adjustment, we may provide adequate climate change information for regional assessment studies.

1. Introduction

It has been well known that the global mean air temperature has been increased gradually since the end of nineteenth century, although there was a cooling period for 1940's to 1970's (IPCC 2001), because of increasing carbon dioxide in the atmosphere. The climate of Korea also has gradually adjusted for the global environmental change. Recently Oh and Kang (2004) reported a significant warming trend in the daily temperature data for 90 years from 1910 to 1999 at Busan weather station (35°6′N, 129°2′E and elevation 69.2 m), which is one of the major synoptic observation sites of the Korea Meteorological Administration (KMA). This warming trend is well illustrated in Fig. 1 in which the annual variations of daily mean temperature in both the 1910's (black line) and 1990's (light line) are compared to demonstrate the relative change in the surface air temperature. Based on the definition of seasons introduced by Oh and Kang (2003), Fig. 1 represents the changes in beginning and ending date of each season in the 1990's, together with those in the 1910's. As shown in Fig. 1, summer has come in advance, and remained later in the 1990's compared to the 1910's. Thus, the length of summer becomes 109 days in the 1990's, while it is 87 days in the 1910's (Table 1). Different from summer, we had short winter nowadays compared to the 1910's. We have only 102 days of winter in the 1990's compared to 129 days in 1910's. Thus, the length of winter is shrunken as much as 27 days. Most of this lost winter days has turned to summer, so that

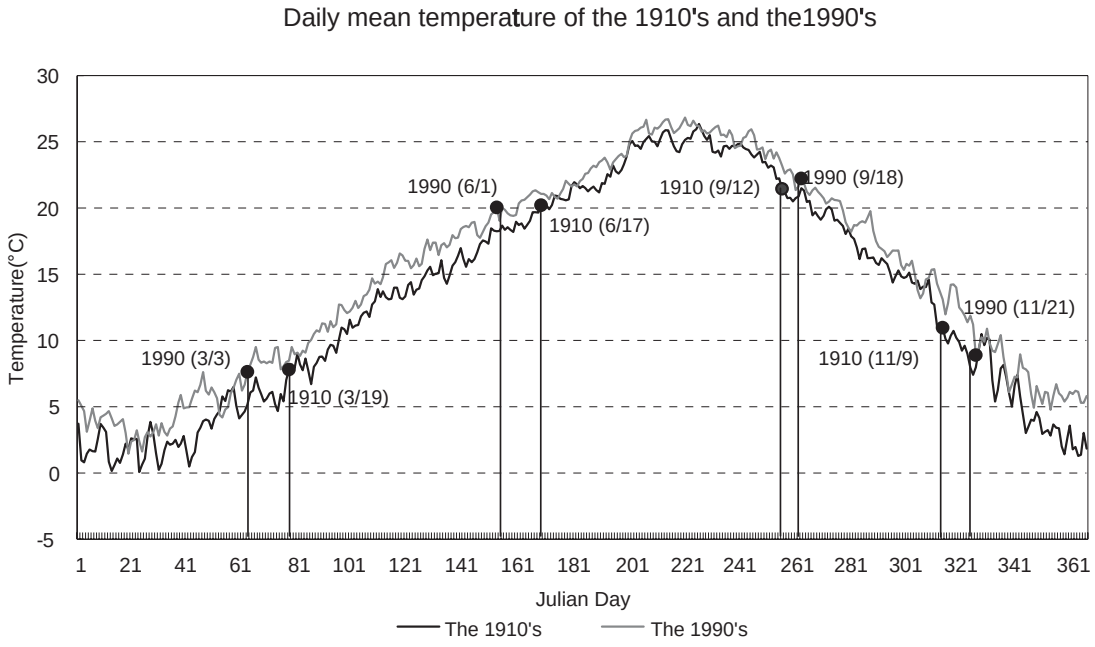

Fig. 1. Variation of daily mean temperature in both 1910's (black line) and 1990's (light line) at Busan together with the beginning and ending of seasons.

Table 1. Change in seasonality between 1910's and 1990's at Busan

	Spring (more than 7.8°C)	Summer (more than 20.0°C)	Autumn (less than 21.8°C)	Winter (less than 11.0°C)
1910's	91 days (March 19∼)	87 days (June 17∼)	58 days (September 12∼)	129 days (November 9∼)
1990's	90 days (March 3∼)	109 days (June 1∼)	64 days (September 18∼)	102 days (November 21∼)
Change in the length of Season	−1 day	+22 days	+6 days	−27 days

summer gains about 22 days as illustrated in Table 1. Spring and autumn are not changed much in terms of length, except the facts that spring starts somewhat earlier, and autumn starts somewhat later compared to the 1910's.

We may observe the evidence of climate changes, not only from the temperature records, but also from the variation in ecosystem. In Korea, during the 15th–19th century, it has been known that the northern limit of bamboo (known as *Phyllostachys*) habitation was about 35°N at the central part of the Korean peninsula, while it reaches as further northward as 38°N in the east coastal region, as shown in Fig. 2 (Gong 2001). By recent field surveys (Oh et al. 2003), however, *Phyllostachys* is found near the 36°N line at the central part of the Korean peninsula, in consequence of recent global warming. Considering that there was a cooling trend for the last thousand years, until the 19th century, Oh et al. (2002) conclude that the habitation of *Phyllostachys* has advanced to northward about 50–100 km during the 20th century. So, if the difference between the present surface air temperature and that of the little ice age of the *Chosun* Dynasty is about 0.6–1.0°C, it is suppose that the boundary of *Phyllostachys* habitation has moved 80–160 km to the northward, per 1°C rise of annual mean surface air temperature. In addition, Oh et al. (2002) found that the boundary of *Phyllostachys* habitation might be controlled by the number of days by which the daily maximum surface air temperature was below the freezing level during January in Korea. It implies how sensitive the habitation of *Phyllostachys* is to temperature changes during the winter season.

Accordingly, it is not easy to derive any solid conclusion on impact assessment for regional climate change, without reasonable and adequate climate information. In this study, we attempt to develop a methodology to provide relatively accurate regional temperature and precipitation information, for not only current climate, but also future climate by combination of dynamical downscaling and statistical adjustment.

2. AOGCM simulations

In order to take into account the internal variability in the inherently chaotic climate system of the numerical models, long-term ensemble simulations are required. Using the AOGCM ECHO-G, we have performed ensemble simulations of climate change for the period 1860–2100 for different greenhouse gas (GHG) scenarios of IPCC SRES (Special Report on Emissions Scenarios, IPCC, 2000) A2 and B2, and recently one simulation has been finished for each scenario.

The AOGCM ECHO-G, which we use in this study, consists of atmospheric component model ECHAM4, and oceanic component model HOPE-G. ECHAM4 is the fourth generation version of the Hamburg atmospheric general circulation model ECHAM, which was modified from ECMWF AGCM for the use of long-term climate simulations (Roeckner et al. 1996b). The T30 grid (∼3.75°) and 19 hybrid sigma-pressure levels are used, which are the same resolution as in a 1000-yr control simulations (hereafter CTL, Baquero-Bernal et al. 2002; Zorita et al. 2003). Ocean model HOPE-G is the global version of the Hamburg Ocean Primitive Equation Model (HOPE), and includes a dynamic-thermodynamic sea-ice model with

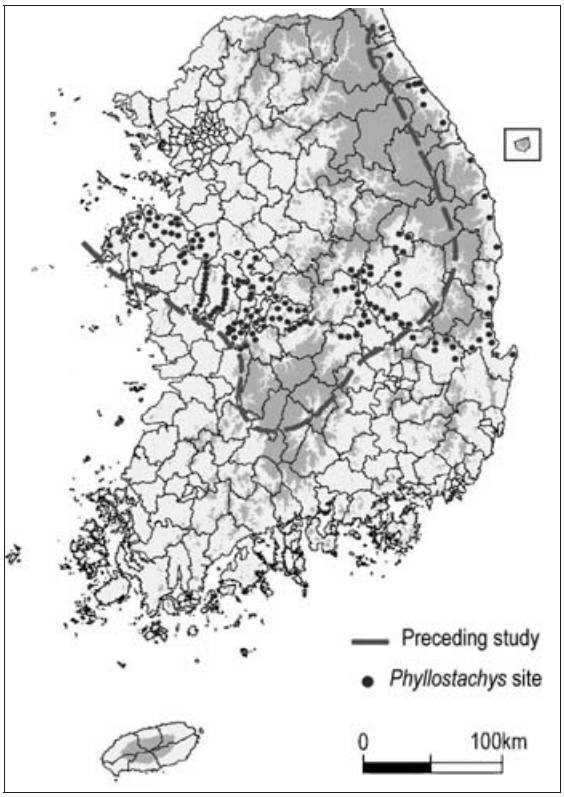

Fig. 2. The comparison for distribution of *Phyllostachys* between preceding study and present in Korea. The grey line is the northern limit of *Phyllostachys* habitation during 15–19th century by (Gong 2001) and the dots represent field survey (Oh et al. 2002).

snow cover. A gaussian T42 grid (about 2.8°) is used, with the meridional refinement of 0.5° in the tropical band between 10°S and 10°N, and vertical resolution is by 20 horizontal layers. ECHAM4 and HOPE-G exchange 10 atmospheric fluxes and 4 ocean and sea-ice information once in a day. Annual mean heat and freshwater fluxes, as diagnosed from the relaxation term during the spin-up, are used as flux corrections. However, no momentum flux corrections are used. This flux correction method has a merit of leaving the seasonal cycle and the wind stress determined by model physics, and has been used in the ECHAM4/OPYC3 whose atmospheric component is the same as that of ECHO-G, except for the different horizontal resolution of T42 gaussian grid (Roeckner et al. 1996a, 1999; Bacher et al. 1998; Stendel et al. 2002). For more details of ECHO-G, see Legutke and Voss (1999).

In climate change simulations with ECHO-G, a total of 19 well-mixed GHGs (greenhouse gases) are used including CO_2, CH_4, N_2O, and industrial halocarbons. GHG concentrations are constructed from observations for the period 1860–1990, and SRES A2 or B2 marker scenarios for the period 1990–2100. These simulations include GHGs only referred to as A2G and B2G, which represent pessimistic and optimistic scenarios, respectively. In the A2G [B2G] scenario, for example, CO_2 concentration increases up to ~821 [~606] ppm by 2100. A2G and B2G are initialized at year 311 of CTL. Because, in CTL, present-day observations are used to estimate flux corrections and spin-up the ocean model and 1990 concentrations of main GHGs (CO_2, CH_4, N_2O) are applied rather than preindustrial ones, there is an initial shift in concentrations of the main GHGs in A2G and B2G. This initial shift is considered by enhancing both the observed and projected concentrations of the main GHGs in an appropriate way by Roeckner et al. (1999). As such, initial warm bias compared to observations, is maintained though the whole simulation, so the derived climate trends are not affected (Roeckner et al. 1999; Stendel et al. 2002).

East Asian (defined as the grid box of 80°E~180°E and 20°N~60°N) climate changes in A2G and B2G, are analyzed focusing on the changes of near surface temperature and precipitation. Analysis results show that East Asia is likely to experience warmer and wetter climate than present, with larger amplitude than global mean (see Fig. 3). The A2G [B2G] result shows ~6.5 [4.5]°C increase of temperature and ~10.5 [6.0]% increase of precipitation over East Asia by 2100, as seen in the lower panels in Fig. 3. However, it should be noted that precipitation projection has a large uncertainty from the dominant interannual and decadal variability, which cannot be reliably estimated from a single realization. Spatial pattern of climate change over East Asia shows that the northern continental area has larger warming than the southern oceanic area, while the precipitation change is dominant over the coastal area of East Asia (see Fig. 4). Local climate change over the Korean Peninsula are projected as about 5~7 [3~5]°C and 10~30

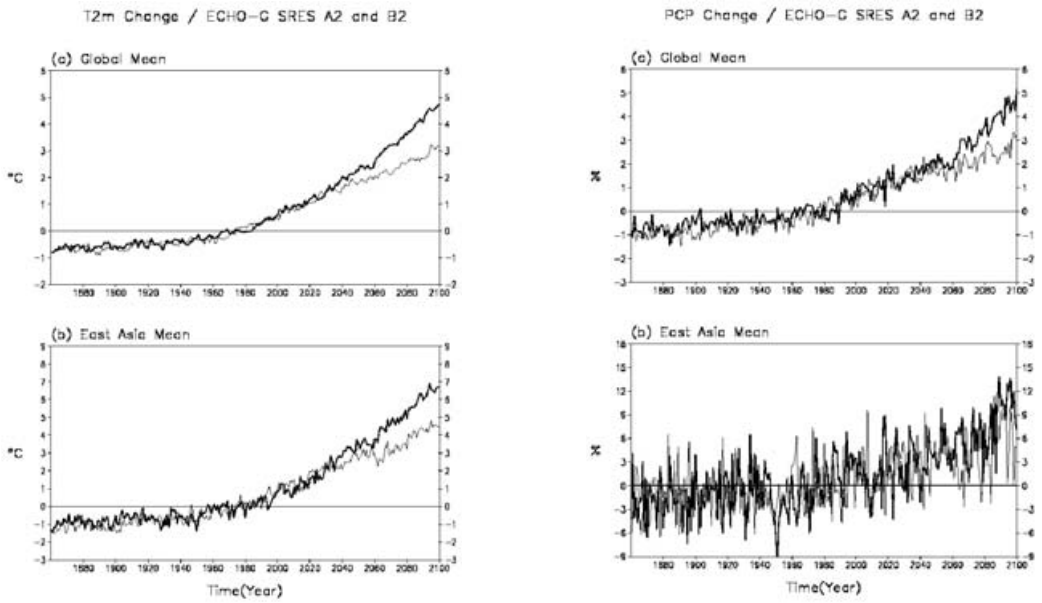

Fig. 3. Time series of annual mean near surface temperature change [°C] (left panels) and precipitation change [%] (right panels) for the period of 1860–2100 in ECHO-G A2G (B2G) simulations: a) globe mean and b) East Asia mean. Thick (thin) solid lines show A2G (B2G) results.

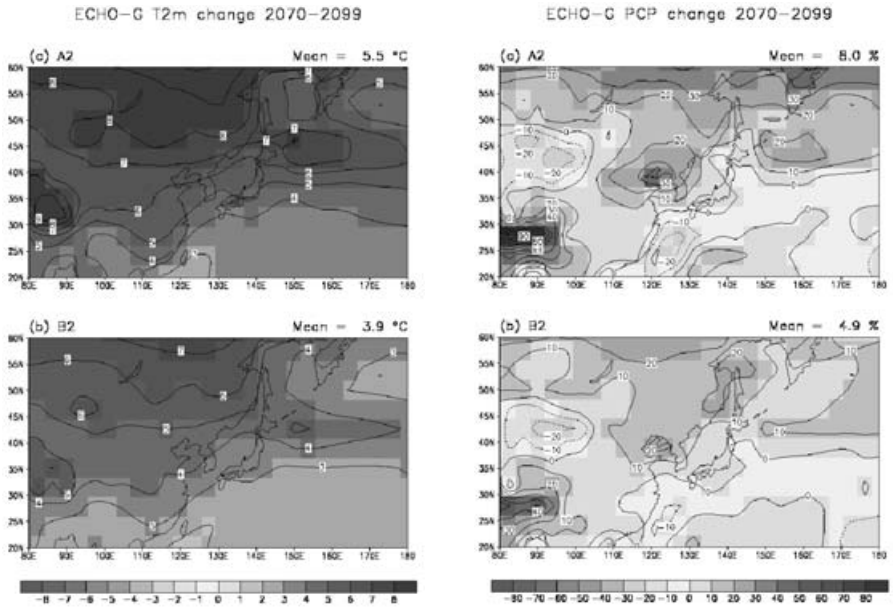

Fig. 4. Climate change patterns over East Asia of temperature [°C] (left panels) and precipitation [%] (right panels) for the period of 2070–2099 in ECHO-G a) A2G and b) B2G simulations. Changes are evaluated from the 30-year mean of 1961–1990. Area-averaged values are shown at the right top of each panel.

[10∼20]% increase in A2G [B2G] by 2100, but large uncertainty should be taken into account. It is interesting to see that there is seasonal dependencies of climate change over East Asia: surface temperature increases in cold season (SON, DJF) are ∼0.5°C stronger than in warm season (MAM, JJA), while precipitation increase in summer (JJA) is dominantly larger than other seasons, which might be related to the strengthening of East Asian summer monsoon system (figures not shown). A precise investigation on the seasonal dependency of climate change might be necessary in the future. It is worthy to note that these analysis results have a large uncertainty, especially in the projection of precipitation change, because only a single realization of ECHO-G is used in the analysis.

3. Dynamic downscaling

Although the resolution of Atmosphere-Ocean General Circulation Models (AOGCMs) is still coarse, simulations of present day climate with the AOGCMs become quite comparable to the observed atmospheric general circulation features in general since the IPCC WGI Second Assessment Report (IPCC, 1996) (hereafter SAR). Meanwhile, the development of high resolution Atmospheric General Circulation Models (AGCMs) shows that the models' dynamics and large-scale flow improve as resolution increases, though this is not uniformly so geographically or across models (e.g., Stratton 1999; Cubasch et al. 1995; Deque and Piedelievre 1995). In some cases, however, systematic errors are worsened compared with coarser resolution models although only very few results have been documented. The direct use of high-resolution versions of current AGCMs, without some allowance of the dependence of models physical parameterizations on resolution, leads to some deterioration in the performance of the models. At the regional scale, in particular, the models display area-average biases that are highly variable from region-to-region and among models, with sub-continental area-averaged seasonal temperature biases typically within 4°C, and precipitation biases mostly between −40 and +80% of observations (IPCC, 2001).

Regional Climate Models (RCMs) based on the concept of "downscaling", implying that the regional climate is conditioned, but not completely determined by the larger scale state, consistently improve the spatial detail of simulated climate compared to General Circulation Models (GCMs) since SAR. The conclusions reported in SAR were that (a) both RCMs and downscaling techniques showed a promising performance in reproducing the regional detail in surface climate characteristics as forced by topography, lake, coastlines and land use distribution; and (b) high resolution surface forcing can modify the climate change signal at the surface on the sub-AOGCM grid scale. RCMs driven by observed boundary conditions show area-averaged temperature biases (regional scales of 10^5 to 10^6 km^2), generally within 2°C, and precipitation biases within 50% of observations (IPCC, 2001).

The nested regional modeling technique essentially originated from numerical weather prediction, and Dickinson et al. (1989) and Giorgi (1990) pioneered the use of RCMs for climate application. RCMs are now used in a wide range of climate applications, from palaeoclimate to anthropogenic climate change studies. They can provide high resolution (up to 10 to 20 km or less) and multi-decadal simulations, and are capable of describing climate feedback mechanisms acting at the regional scale. A number of widely used limited area modeling systems have been adapted to, or developed for, climate application. More recently, RCMs have begun to couple atmospheric models with other climate process models, such as hydrology, ocean, sea-ice, chemistry/aerosol and land-biosphere models.

One of the important issues in long-term integrations using dynamic downscaling method is nesting of RCMs to coarse large-scale domain, to prevent long-term drift between the solutions of the coarse and nested domains. Hong and Juang (1998) demonstrated that regional model forecasts are consistent with coarse model forecasts without a discernible systematic bias, by introducing a simple orography blending technique near the lateral boundary of the regional model, with that of a coarse model. A similar linear orography blending method has been adopted for long-term integration of RCM. For a regional climate simulation, MM5 (version 3.4) with 27 km horizontal resolution, and 18 layers of σ-

Table 2. List of ECHO-G variables used to the initial and lateral boundary conditions for RCM (MM5)

Variable	Unit
U-velocity	[m/s]
V-velocity	[m/s]
Temperature	[K]
Specific humidity	[kg/kg]
Sea level pressure	[Pa]
Geopotential height	[gpm]

coordinate in vertical, is nested within the output of IPCC SRES A2 experiment, provided by the AOGCM ECHO-G for the period of model year 2001 to 2030 (details are in Oh et al. 2002).

In the regional simulations, the MM5 was driven by updating the lateral boundary conditions at 4-hour intervals using the interpolated ECHO-G data. Its lateral boundary conditions, such as sea level pressure (Pa), the longitudinal and latitudinal wind (m/s), specific humidity (kg/kg), temperature (K) and geopotential height (gpm) as listed in Table 2. Figure 5 shows the time series of monthly mean air temperature for East Asia, simulated by both AOGCM ECHO-G and MM5 for 30 years from 2001 to 2030. The time series of air temperature simulated by MM5 has followed that of AOGCM ECHO-G, however, the cold bias has been found in the simulation by MM5 compared to AOGCM ECHO-G. This cold bias has a tendency to be shrunken during the summer season and enlarged during the winter season (Fig. 5). Although the nested model has tried to catch up, the initial cold bias through integration is so slow that the bias may remain at least for a significant period in the 100 years integration. It can be mislead when the MM5 output is used in the studies on regional climate change assessment without adequate treatment. We will discuss this matter in detail at section 4.

The left panels in Fig. 6 show the seasonal mean air temperature in East Asia by the GCM (upper) and RCM (MM5) (lower), respectively. The results of RCM are quite similar to those of GCM, except regional details mostly come from detail topography used in RCM. For summer, (JJA) significant warming in south China in large-scale climate data by AOGCM has been removed by RCM. In addition, RCM produces surface air temperature at mountainous region more realistically than AOGCM. A similar conclusion can be derived from other seasons. The cold area in northern Majuria has expended to further south in RCM compared to AOGCM. These are highly encouraging features for the

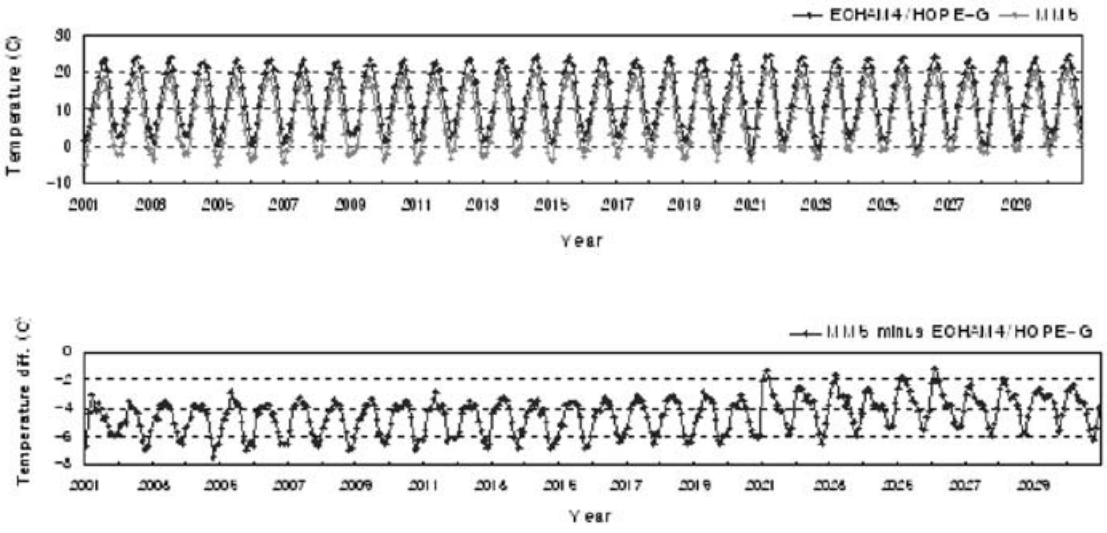

Fig. 5. Time series of surface air temperature simulated by both AOGCM and MM5 (upper panel) together with their difference (MM5—AOGCM) (lower panel) for the period from model year 2001 to 2030.

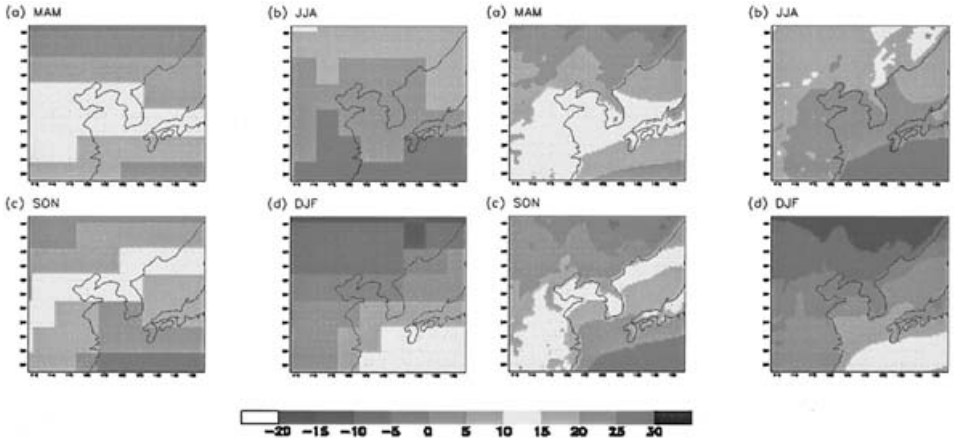

Fig. 6. Seasonal temperature change [°C] for the model year 2001 to 2030 by both GCM (left panels) and RCM (right panels) for (a) MAM, (b) JJA, (c) SON, and (d) DJF, respectively.

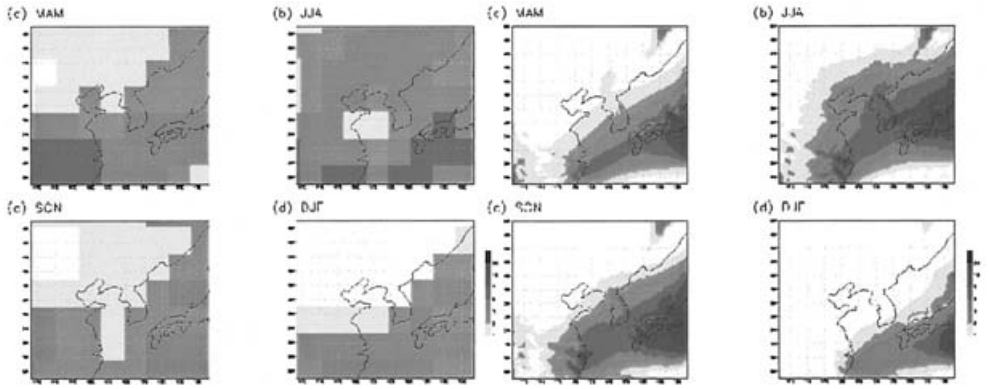

Fig. 7. Seasonal precipitation change [%] for the model year 2001 to 2030 by both GCM (left panels) and RCM (right panels) for (a) MAM, (b) JJA, (c) SON, and (d) DJF, respectively.

studies on the impact assessment for climate change. We may reach to the same conclusion with precipitation simulations. Similar to temperature changes, the right panels in Fig. 6 present the seasonal precipitation changes (%) for the model year 2001 to 2030 by GCM (upper) and RCM (lower), respectively. For all seasons, the development of monsoon is well organized in the RCM simulation compared to that in GCM. In the right upper panel in Fig. 7, we hardly have to see such an organized monsoon development, mainly due to its coarse horizontal resolution. Another distinguished feature is that there is less precipitation in the northern and eastern part of East Asia. We could not find any particular cause for this feature, however, we suspect a boundary problem in nesting.

4. Statistical adjustment

Transfer function approaches have subsequently emerged to satisfy the need to correct the systematic bias of dynamic model in the regional-scale, or to predict the regional climate from large-scale predictors (Kim et al. 1984; Wigley et al. 1990; Wilby et al. 1998; Kim et al. 2004). Fundamental to this approach is the assumption that stable empirical relationships can be established between atmospheric processes occurring at disparate temporal and/or spatial scales (Wilby et al. 1998). A major part of this systematic error can be corrected by the statistical relationship between model data and observed data, the so-called principal

component analysis such as coupled pattern technique, regression analysis and empirical orthogonal function analysis (EOFA). Most commonly used methodologies of the coupled pattern technique are based on singular value decomposition analysis (SVDA), and canonical correlation analysis (CCA). Ward and Navarra (1997) applied SVDA to simultaneous fields of GCM simulated precipitation and observed precipitation to correct the errors in model response to SST forcing. A recent study by Feddersen et al. (1999) demonstrated, however, that the post-processed results are not sensitive to the choice among the methods based on the CCA, SVD, and EOFA. In this study, the systematic bias of RCM was corrected by the transfer function, which is constructed by EOFA and simple linear regression analysis.

a. Methodology of adjustment for systematic bias

The observed data used in this study are the daily mean temperature of 17 surface observation stations in Korea for 10 years from 1992 to 2001, and two 10-year simulation data obtained from a regional climate model (RCM), with the period 1992–2001 and 2021–2030. Based on the empirical orthogonal function analysis (EOFA), and simple linear regression analysis, the transfer functions are obtained for each mode of EOFA to correct the systematic bias of RCM data.

Let $X(x,t)$ and $Y(y,t)$ be RCM data, and the observed data with time (t) and space (x or y), respectively where $x(y)$ are from 1 to $p(q)$. p and q are the number of grid point in RCM and station in observation, respectively. The representation of the data are as follows, based on EOFA

$$X(x,t) = \sum_{i=1}^{P} e_i^m(x) T_i^m(t) \tag{1}$$

$$Y(y,t) = \sum_{i=1}^{q} e_i^o(y) T_i^o(t) \tag{2}$$

where e_i and T_i indicate the eigen vector and normalized time coefficient of each mode, respectively. The superscript o and m indicate the observation and model, respectively.

The first step is to find the main modes with the similar dynamical origin, such as seasonal cycle in both sides from EOFA. Then the second step is to obtain the relationship between $T_i^m(t)$ and $T_i^o(t)$ for each mode from simple linear regression analysis.

$$TE_i^o(t) = \beta_{0i} + \beta_{1i} T_i^m(t) \tag{3}$$

where β_{0i} and β_{1i} indicate regression coefficients of each mode i. $TE_i^o(t)$ means the estimated time coefficients of $T_i^o(t)$. The third step is to reconstruct the corrected distribution using equation (4).

$$C(y,t) = \sum_{i=1}^{q} e_i^o(y) TE_i^o(t) \tag{4}$$

where $C(y,t)$ indicates the corrected value of RCM data. The final bride to complete the transfer function is equation (5), which provides the bridge to obtain $TE_i^o(t)$ in equation (3) for given $X(x,t)$.

$$T_i^m(t) = \sum_{x=1}^{p} X(x,t) e_i^m(x) \tag{5}$$

We named these procedures Empirical Orthogonal Transfer function (EOTF) method. If we can obtain the transfer function between the observation and RCM data for the training period like the control run, the corrected RCM output will be able to obtain from RCM data for the CO_2 increasing condition based on the EOFT method. The credibility of this method depends on the strong relationship between the observation and Model data in the leading eigen modes of EOFA.

b. Application to RCM data

In application, we obtained the leading two modes from EOFA for daily mean temperature in Korea. In observation the eigen vector of the first mode has the positive sign in all the regions, but larger value toward inland than along the coast, indicating that the seasonal cycle has large amplitude inland (Fig. 8a). The first mode shows the seasonal cycle, with strong positive signal in August and negative signal in February (Fig. 8b). The second mode shows another seasonal cycle related to the ocean effect (Figs. 8c, d). The eigen vector of the second mode has the east-west pattern with the positive value along the coast, and negative value toward inland (Fig. 8c). The amplitude of

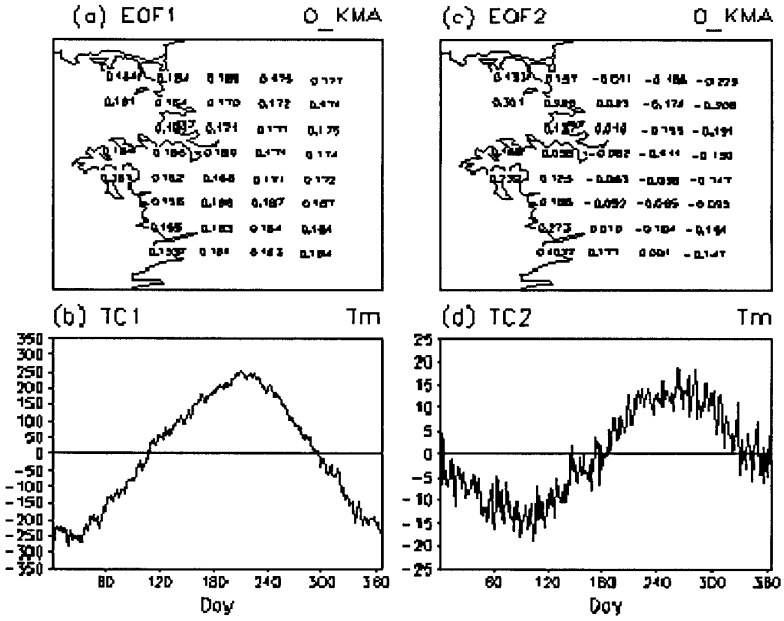

Fig. 8. (a) The first and (c) second eigen vector of EOFA for the observed daily mean temperature. The lower panels are the associated time coefficients of the first and second modes, respectively.

the second mode shows the seasonal cycle, with the positive peak in September and the negative peak in March, indicating that the phase of the second mode is delayed about one month compared to the first mode (Figs. 8b, d). The second mode explains that the coastal region has warming in the period from July to November and cooling in the period from December to June, by the influence of the Yellow sea. Nevertheless, the inland region is reversed with the opposite sign. In the temperature by RCM (Fig. 9), the eigen modes are very similar to the observational modes, implying that RCM can simulate the variability in observation reasonably. However, the amplitude of time coefficient has some difference. The amplitude of RCM seasonal cycle shows larger than the observation, but the similar phase between the two modes. These characteristics means that the transfer function between the observation, and RCM temperature, can be easily constructed using the modes with the same dynamic origin.

For the leading two modes, the amplitude of normalized time coefficients in RCM temperature is much bigger than in observation data, but the phases are very similar (Fig. 10b, Fig. 11b). As shown in Figs. 8 and 9, the eigen vector patterns in the upper two modes for RCM data are very similar to those for observation data, indicating that stable empirical relationships can be established between atmospheric processes occurring at disparate temporal and/or spatial scales. Based on the above characteristics, the regression coefficients have been obtained using the normalized time coefficients of EOFA (Figs. 10a, 11a). The regression coefficients β_{1i} in the first two modes are 0.38938, and 0.33244, respectively. Nevertheless, when $T_i(t)$ is dimensionless, normalized anomaly time series, the intercept β_{0i} in the leading two modes are zero, because of the same phase of the time coefficients in the observation and RCM. The coefficients of determination R^2 in the regression analysis for the leading two modes are 0.98, 0.81, respectively, indicating that this empirical orthogonal transfer function method is quite acceptable even in the daily time scales.

Figure 12a shows the RMS (root mean square) error between the observation and RCM in the daily time scale during the spring season. The RMS error is smaller along the coastal region than toward inland with the range from 10°C to 2°C, implying that the error was originated from the effect of topography.

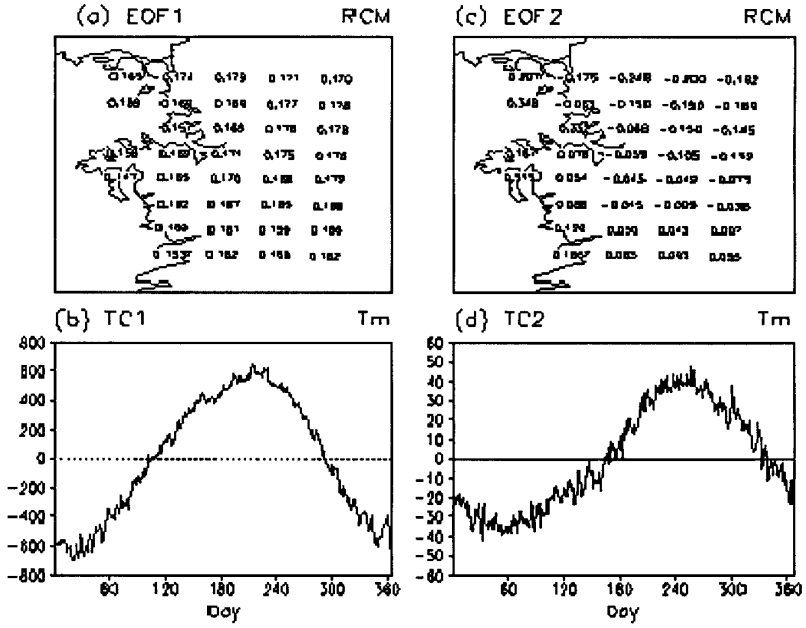

Fig. 9. Same as in Fig. 8 except for the RCM daily mean temperature.

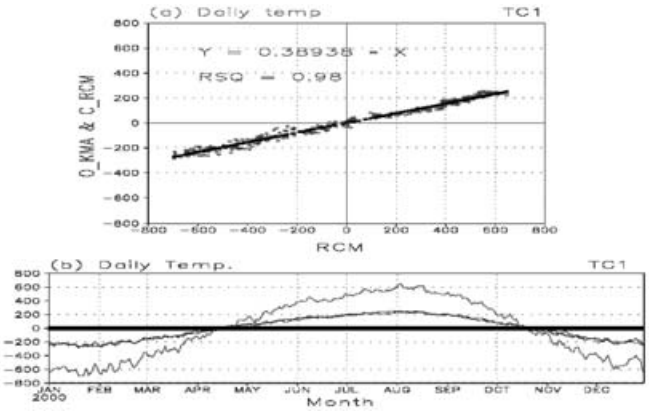

Fig. 10. (a) Scatter diagram of the time coefficients of the first mode in EOFA between RCM and observation for daily mean temperature in Korea. The regression line (solid line), equation and the coefficient of determination (RSQ) are also indicated in (a). (b) As in (a) except for the time series. The lines in (b) indicate RCM, observation and the correction by transfer function, respectively.

The RMS error is significantly reduced after correcting the systematic bias based on the transfer function. It is below 2°C, even in the largest error region (Fig. 12a). The distribution of RMS error in the summer is quite similar to that in the spring expect for the largest RMS error among the all season, with the range from 3 to 17°C (Fig. 12b). The corrected RMS error has the range from 0.8 to 2.5°C, which is just about 5–20% of the original RMS error (Fig. 12b). The RMS error patterns in fall and winter are very similar to these in summer and spring, indicating that the RMS error is systematic, thus to be corrected (Figs. 12c, d). The RMS error after the correction is very small compared to the original RMS error. It is below 2°C in the annual mean.

The effect of correction using the transfer

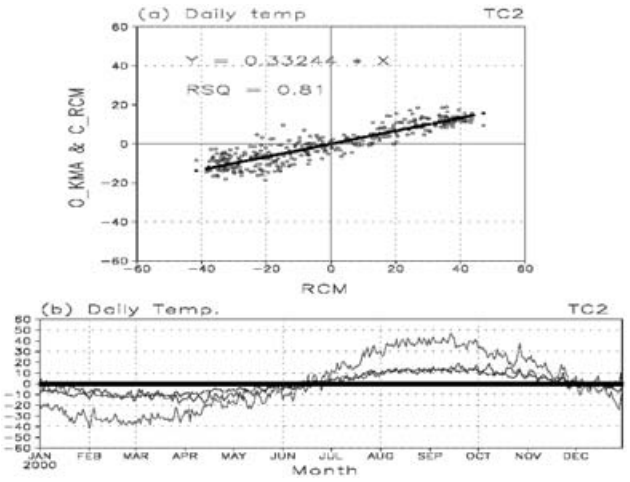

Fig. 11. Same as in Fig. 10 except for the second mode.

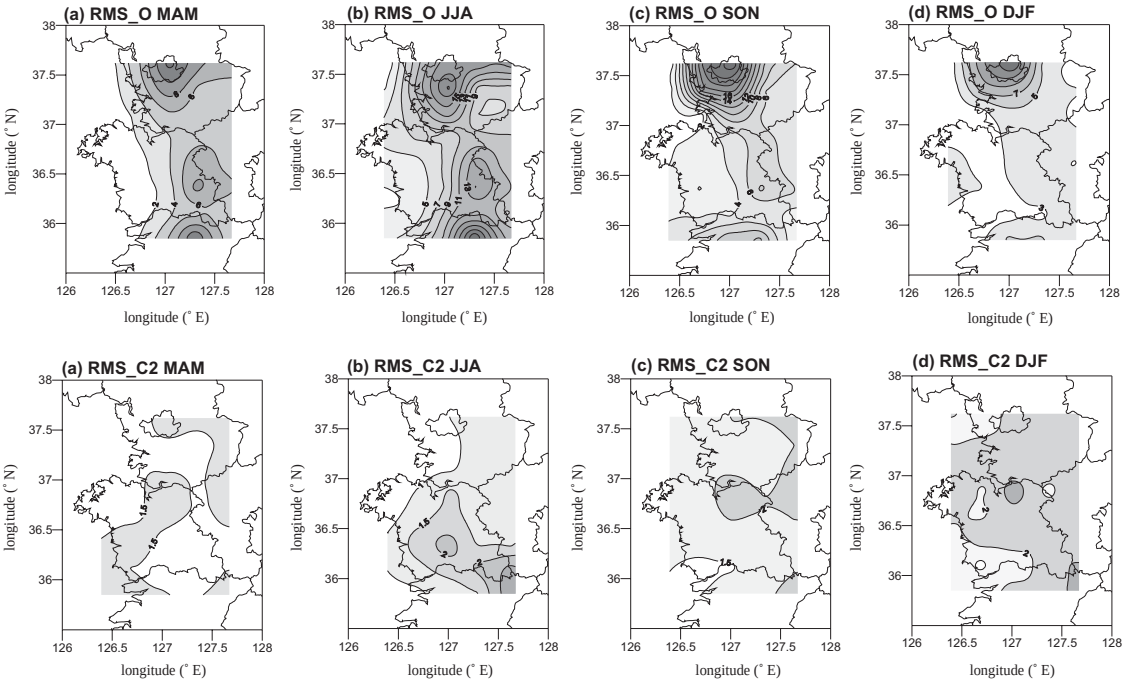

Fig. 12. Root mean square error of daily mean temperature in RCM (upper panels) and C-RCM (lower panels) for (a) MAM, (b) JJA, (c) SON, and (d) DJF, respectively. C-RCM indicates RCM after correcting the systematic bias using the empirical orthogonal transfer function (EOFT) method developed by this study. Contour intervals in the upper and lower panels are 2 and 0.5°C, respectively.

Table 3. RMS error (°C) of daily mean temperature in Korea. RCM_C1 and RCM_C12 indicate RMS errors after correcting the first mode and the leading two modes, respectively.

RMS error season	RCM	RCM_C1	RCM_C12	Corrected percentage (%)
spring	4.73	1.78	1.48	68.7
summer	9.70	1.45	1.31	86.5
autumn	6.64	2.20	1.86	72.0
winter	4.03	2.16	2.11	47.6
annual	6.29	1.90	1.69	73.1

function is summarized in Table 3. RMS error of the daily mean temperature in RCM used has the range from 4.03 in winter to 9.70°C in summer, the biggest cold bias in summer. RMS error of daily mean temperature in RCM is significantly reduced after a correction based on the transfer function. Corrected percentage in RMS error has the range from 47.6 in winter to 86.5% in summer, indicating that the empirical orthogonal transfer function (EOTF) method, developed in this study, is very useful even in daily time scale. But, climate change mostly means the difference, not the variable values themselves, implying that systematic bias may cancel between different periods. Table 4 shows the difference between with adjustment, and without adjustment in daily mean temperature. Actually the difference in climate change between the two methods is reduced in comparison with the difference in the current climate. The difference between two climate changes has the range from −8.7% in fall to 28.8% in winter, relative to the temperature change from dynamic downscaling. These results suggest that although systematic bias can cancel between two periods, statistical adjustment is also important to reduce the model bias.

5. Conclusion

By combining dynamic downscaling and statistical adjustment, we may provide reasonable future regional climate information from global climate model simulations. The final output of temperature is quite adequate for regional assessment studies change, since there are distinguished variation modes influenced by land and ocean. Precipitation, however, has a lot of room to be improved. There are somewhat disagreement in dominant modes of real world and model world. This may be caused not only from the fact that precipitation is a local phenomena, and less systematic than temperature, but also the model has still treated the precipitation processes inadequately. This might be one of important tasks of future studies, to overcome and provide reasonable regional climate change information.

Through this study, we have learned that the adjustment of land surface temperature takes quite a long period. The cold bias generated by the RCM has remained, with almost the original gap through 30 years integration. Accordingly, it might be necessary to apply the spin-up procedure for land surface in the RCM, before long-term integration. It may provide more reasonable regional climate change information, and less statistical adjustment.

Acknowledgement

The authors are grateful to reviewers for their helpful comments on the manuscript. This research was performed as a project of the Korean Meteorological Research Institute, "Re-

Table 4. The difference between statistical adjustment and dynamic downscaling in the daily mean temperature change between 1992–2002 and 2021–2030. The difference is indicated as the percentage relative to dynamic downscaling.

difference	spring	summer	autumn	winter	annual
Minimum	−14.9	−12.3	−8.7	−17.2	−12.5
Maximum	17.8	15.2	10.6	28.8	13.4

search on the Development of Regional Climate Change Scenarios to Prepare the National Climate Change Report (I)."

References

Bacher, A., J.M. Oberhuber and E. Roeckner, 1998: ENSO dynamics and seasonal cycle in the tropical Pacific as simulated by the ECHAM4/OPYC3 coupled general circulation model. *Clim. Dyn.*, **14**, 431–450.

Baquero-Bernal, A., M. Latif and S. Legutke, 2002: On dipolelike variability of sea surface temperature in the tropical Indian Ocean. *J. Climate*, **15**, 1358–1368.

Cubasch, U., J. Waszkewitz, G. Hegerl and J. Perlwitz, 1995: Regional climate changes as simulated in time-slice experiments. *Clim. Change*, **31**, 273–304.

Deque, M. and J.P. Piedelievre, 1995: High resolution climate simulation over Europe. *Clim. Dyn.*, **11**, 321–339.

Dickinson, R.E., R.M. Errico, F. Giorgi and G.T. Bates, 1989: A regional climate model for western United States. *Clim. Change*, **15**, 383–422.

Feddersen, H., A. Navarra and M.N. Ward, 1999: Reduction of model systematic error by statistical correction for dynamic seasonal prediction. *J. Climate*, **12**, 1974–1989.

Giorgi, F., 1990: Simulation of regional climate using a limited area model nested in a general circulation model. *J. Climate*, **3**, 941–963.

Gong, W.S., 2001: Temporal and spatial changes in the distribution of *Phyllostachys* habitation. *Kor. Geograph. Soc.*, **36**, 444–457 (in Korean).

Hong, S.-Y. and H.-M. Juang, 1998: Orography blending in the lateral boundary of a regional model. *Mon. Wea. Rev.*, **126**, 1714–1718.

IPCC, 1996: *Climate change 1995: The Science of Climate Change*. Contribution of Working Group I to the Second Assessment Report of the Intergovernmental Panel on Climate Change [J.T. Houghton, L.G. Meira Filho, B.A. Callander, N. Harris, A. Kattenberg and K. Maskell (eds.)], Cambridge University Press, Cambridge, 572pp.

IPCC, 2000: *Special Report on Emissions Scenarios*, Nakicenovic, Nebojsa and Swart, Rob (eds.), Cambridge University Press, Cambridge, United Kingdom, 612pp.

IPCC, 2001: *Climate Change 2001: The Scientific Basis*. Contribution of Working Group I to the Third Assessment Report of the Intergovernmental Panel on Climate Change (IPCC) J.T. Houghton, Y. Ding, D.J. Griggs, M. Noguer, P.J. van der Linden and D. Xiaosu (Eds.) Cambridge University Press, UK. 944pp.

Kim, J.W., J.T. Chang, N.L. Barker, D.S. Wilks and W.L. Gates, 1984: The statistical problem of climate inversion: Determination of the relationship between local and large-scale climate. *Mon. Wea. Rev.*, **112**, 2069–2077.

Kim, M.-K., I.-S. Kang, C.-K. Park and K.M. Kim, 2004: Super ensemble prediction of regional precipitation over Korea. *Intl. J. Climatol.*, **24**, 777–790.

Legutke, S. and R. Voss, 1999: *The Hamburg atmosphere-ocean coupled circulation model ECHO-G*. Technical report No. 18, German Climate Computer Center (DKRZ), Hamburg, Germany, 62pp.

Oh, J.-H. and D.-Y. Kang, 2004: Climate change during 20th century at Busan, Korea (which can be obtained by e-mail to jhoh@pknu.ac.kr) (to be submitted).

Oh, J.-H., M.-K. Kim, S.-H. Lee and T.-K. Kim, 2002: "*Development on regional climate change scenarios for Korea peninsula and East Asia*", Meteorological Research Institute, KMA, Seoul, Korea, 212pp (in Korean) (which can be obtained by e-mail to jhoh@pknu.ac.kr).

Roeckner, E., J.M. Oberhuber, A. Bacher, M. Christoph, I. Kirchner, 1996a: ENSO variability and atmospheric response in a global coupled atmosphere-ocean GCM. *Clim. Dyn.*, **12**, 737–754.

Roeckner, E., K. Arpe, L. Bengtsson, M. Christoph, M. Claussen, L. Dümenil, M. Esch, M. Giorgetta, U. Schlese and U. Schulzweida, 1996b: *The atmospheric general circulation model ECHAM-4: model description and simulation of present-day climate*. Report No. 218, the Max Planck Institute for Meteorology, Hamburg, Germany.

Roeckner, E., L. Bengtsson and J. Feichter, 1999: Transient climate change simulations with a coupled atmosphere-ocean GCM including the tropospheric sulfur cycle. *J. Climate*, **12**, 3004–3032.

Stendel, M., T. Schmith, E. Roeckner and U. Cubasch, 2002: *The climate of the 21st century: Transient simulations with a coupled atmosphere-ocean general circulation model*. Revised version, Climate Centre Report 02-1, Danish Meteorological Insitute, Denmark, 50pp.

Stratton, R.A. 1999: A high resolution AMIP integration using the Hadley Centre model HadAM2b. *Clim. Dyn.*, **15**, 9–28.

Ward, M.N. and A. Navarra, 1997: Pattern analysis of SST-forced variability in ensemble GCM

simulations: Examples over Europe and tropical Pacific. *J. Climate*, **10**, 2210–2220.

Wigley, T.M.L., P.D. Jones, K.R. Briffa and G. Smith, 1990: Obtaining sub-grid-scale information from coarse-resolution general circulation model output. *J. Geophys. Res.*, **95(D2)**, 1943–1953.

Wilby, R.L., T.M.L. Wigley, D, Conway, P.D. Jones, B.C. Hewitson, J. Main and D.S. Wilks, 1998: Statistical downscaling of general circulation model output: A comparison of methods. *Water. Resour. Res.* **33(11)**, 2995–3008.

Zorita, E., F. González-Rouco and S. Legutke, 2003: Testing the Mann et al. (1998) approach to paleoclimate reconstructions in the context of a 1000-yr control simulation with the ECHO-G coupled climate model. *J. Climate*, **16**, 1378–1390.